Journal of Sound and Vibration 433 (2018) 248–264

Contents lists available at ScienceDirect

Journal of Sound and Vibration

journal homepage: www.elsevier.com/locate/jsvi

Reduced-order modelling of wave propagation in an elastic layer of constant curvature and thickness

S.V. Sorokin [a,*], C.J. Chapman [b]

[a] Department of Materials and Production, Aalborg University, Fibigerstraede 16, DK 9220 Aalborg, Denmark
[b] Department of Mathematics, University of Keele, Keele, Staffordshire, ST5 5BG, United Kingdom

ARTICLE INFO

Article history:
Received 23 November 2017
Received in revised form 18 May 2018
Accepted 9 July 2018

Handling Editor: G. Degrande

Keywords:
Curved elastic layer
Wave propagation
Reduced-order modelling
Accuracy assessment

ABSTRACT

This paper is concerned with reduced-order modelling of wave propagation in an elastic layer of constant curvature and thickness by means of the generalised Galerkin method with Legendre polynomials used as coordinate functions. A new family of polynomial approximations to the dispersion relation and corresponding approximations to the field variables are obtained. These approximations have high accuracy, particularly in resolving the surface waves which are dominant features of the solution. The convergence rate is assessed by alternative accuracy measures and shown to be exponentially fast while the order of polynomials increases at a slow and regular rate. Detailed analysis of displacements and stresses in (frequency, wavenumber) space is performed. This novel modelling should facilitate studies of mode conversion around bends, where short waves are involved, for example in soft materials.

1. Introduction

The analysis of wave propagation in an elastic layer of constant curvature and thickness is an ideal benchmark problem to assess accuracy and efficiency of various approximate theories and methods. The exact solutions in the plane strain case are readily available for a straight layer [1,2] and for a 'thick-walled hollow cylinder' [3]. The theories, or models, of Bernoulli-Euler, Mindlin-Herrmann and Timoshenko are generally recognized as 'low frequency – long wave' approximations of the exact Rayleigh-Lamb solution. The thin shell approximation referred to in the literature as a curved beam theory [2,4,5] is also known as a 'low frequency – long wave' approximation of the exact solution of the problem for a layer of constant curvature.

Recently, a hierarchy of reduced-order models of elastic wave propagation in a straight layer have been formulated in Refs. [6,7] to capture as many branches of dispersion diagram as necessary. The two distinctive features of these models are that the dispersion equations are formulated as low-order polynomials in both frequency and wavenumber and that the cut-on frequencies match their exact counterparts. The idea of the present paper is to formulate similar hierarchy for a layer of constant curvature and to assess ranges of validity of its members. However, the methodology employed here differs profoundly from those used in Refs. [6,7]. The point of departure is the energy functional, and the variational method, often referred to as the generalised Galerkin's method [8,9] is used with the Legendre polynomials as the coordinate functions. By these means, the governing differential equations, which provide a polynomial dispersion equation at any approximation level, are derived. Although this methodology is described both in the context of alternative projection methods [10] and in

* Corresponding author.
E-mail addresses: svs@m-tech.aau.dk (S.V. Sorokin), c.j.chapman@maths.keele.ac.uk (C.J. Chapman).

https://doi.org/10.1016/j.jsv.2018.07.018
0022-460X/

the context of the finite element method [11, Chapter 3], it has not yet been, to the best of our knowledge, used for analysis of elastic wave propagation.

The derivation of governing equations is presented in Section 2. The alternative convergence and accuracy measures are introduced and discussed in Section 3. Section 4 is concerned with analysis of dispersion diagrams, obtained at different approximation levels. The detailed field analysis and convergence studies are presented in Section 5. Results of studies are summarized in Conclusions.

2. Governing equations of generalised Galerkin method

The equations of the generalised Galerkin's method for a curved layer of constant curvature and thickness may be obtained straightforwardly from the governing differential equations of motion and the traction-free boundary conditions. However, we derive here these equations from Hamilton principle in order to highlight the variational nature of this method in elasto-dynamics.

We consider the plane strain state of a layer. Its thickness h is chosen as a length scale, and stresses are scaled by ρc_2^2. Here ρ is the material density, and (c_1, c_2) are the (P, S) wave speeds. The scaled radius of curvature of the centreline of a layer is designated as r_0. The scaled displacement in the circumferential direction (along the θ- axis) is $\tilde{u}(r, \theta, t)$, the scaled displacement in the radial direction (along the r- axis) is $\tilde{v}(r, \theta, t)$. The analysis is restricted to free wave propagation in the absence of external forces.

The kinetic energy is:

$$T = \frac{1}{2}\rho h^4 \int_{r_0-1/2}^{r_0+1/2} \int_{\theta_1}^{\theta_2} \left[\left(\frac{\partial \tilde{u}(r,\theta,t)}{\partial t} \right)^2 + \left(\frac{\partial \tilde{v}(r,\theta,t)}{\partial t} \right)^2 \right] r dr d\theta \tag{1}$$

The potential energy is (here $\alpha = \frac{c_1}{c_2}$):

$$V = \frac{1}{2}\rho h^2 c_2^2 \int_{r_0-1/2}^{r_0+1/2} \int_{\theta_1}^{\theta_2} \left[\left(\alpha^2 \frac{\partial \tilde{u}(r,\theta,t)}{\partial r} + \left(\alpha^2 - 2\right) \frac{1}{r} \left(\frac{\partial \tilde{v}(r,\theta,t)}{\partial \theta} + \tilde{u}(r,\theta,t) \right) \right) \frac{\partial \tilde{u}(r,\theta,t)}{\partial r} + \left(\alpha^2 \frac{1}{r} \left(\frac{\partial \tilde{v}(r,\theta,t)}{\partial \theta} + \tilde{u}(r,\theta,t) \right) \right.$$
$$\left. + \left(\alpha^2 - 2\right) \frac{\partial \tilde{u}(r,\theta,t)}{\partial r} \right) \frac{1}{r} \left(\frac{\partial \tilde{v}(r,\theta,t)}{\partial \theta} + \tilde{u}(r,\theta,t) \right) + 2 \left(r \frac{\partial}{\partial r} \left(\frac{\tilde{v}(r,\theta,t)}{r} \right) + \frac{1}{r} \frac{\partial \tilde{u}(r,\theta,t)}{\partial \theta} \right)^2 \Bigg] r dr d\theta \tag{2}$$

These formulas are substituted in the action integral $H = \int_{t_1}^{t_2} [T - V] dt$, variation $\delta H = 0$ is taken and standard by-parts integration is performed. Then time dependence is taken as $\exp(-i\omega t)$, i.e. $\tilde{u}(r, \theta, t) = u(r, \theta)\exp(-i\omega t)$, $\tilde{v}(r, \theta, t) = v(r, \theta)\exp(-i\omega t)$, this multiplier is omitted and the frequency parameter is introduced as $\Omega = \frac{\omega h}{c_1}$. The system of two variational equations is obtained by equating to zero expressions containing the independent variations $\delta u(r, \theta)$ and $\delta v(r, \theta)$:

$$\int_{r_0-1/2}^{r_0+1/2} \int_{\theta_1}^{\theta_2} \left[\Omega^2 u(r,\theta) + \frac{\partial \sigma_{rr}(r,\theta)}{\partial r} + \frac{1}{r} \frac{\partial \sigma_{r\theta}(r,\theta)}{\partial \theta} + \frac{1}{r} \left(\sigma_{rr}(r,\theta) - \sigma_{\theta\theta}(r,\theta) \right) \right] \delta u(r,\theta) r dr d\theta - \int_{\theta_1}^{\theta_2} \sigma_{rr}(r,\theta) \delta u(r,\theta) r \Big|_{r=r_0-1/2}^{r=r_0+1/2} {}_{2d\theta=0} \tag{3a}$$

$$\int_{r_0-1/2}^{r_0+1/2} \int_{\theta_1}^{\theta_2} \left[\Omega^2 v(r,\theta) + \frac{\partial \sigma_{r\theta}(r,\theta)}{\partial r} + \frac{1}{r} \frac{\partial \sigma_{\theta\theta}(r,\theta)}{\partial \theta} + \frac{2\sigma_{r\theta}(r,\theta)}{r} \right] \delta v(r,\theta) r dr d\theta - \int_{\theta_1}^{\theta_2} \sigma_{r\theta}(r,\theta) \delta v(r,\theta) r \Big|_{r=r_0-1/2}^{r=r_0+1/2} {}_{2d\theta=0} \tag{3b}$$

Non-dimensional stresses in Eq (3) are:

$$\sigma_{rr}(r,\theta)=\alpha^2\frac{\partial u(r,\theta)}{\partial r}+\left(\alpha^2-2\right)\frac{1}{r}\left(\frac{\partial v(r,\theta)}{\partial\theta}+u(r,\theta)\right)$$
$$\sigma_{\theta\theta}(r,\theta)=\alpha^2\frac{1}{r}\left(\frac{\partial v(r,\theta)}{\partial\theta}+u(r,\theta)\right)+\left(\alpha^2-2\right)\frac{\partial u(r,\theta)}{\partial r} \tag{4}$$
$$\sigma_{r\theta}(r,\theta)=2\left(r\frac{\partial}{\partial r}\left(\frac{v(r,\theta)}{r}\right)+\frac{1}{r}\frac{\partial u(r,\theta)}{\partial\theta}\right)$$

The Eq (3) yield the canonical differential equations of motion for a curved layer

$$\Omega^2u(r,\theta)+\frac{\partial\sigma_{rr}(r,\theta)}{\partial r}+\frac{1}{r}\frac{\partial\sigma_{r\theta}(r,\theta)}{\partial\theta}+\frac{1}{r}(\sigma_{rr}(r,\theta)-\sigma_{\theta\theta}(r,\theta))=0 \tag{5a}$$

$$\Omega^2v(r,\theta)+\frac{\partial\sigma_{r\theta}(r,\theta)}{\partial r}+\frac{1}{r}\frac{\partial\sigma_{\theta\theta}(r,\theta)}{\partial\theta}+\frac{2\sigma_{r\theta}(r,\theta)}{r}=0 \tag{5b}$$

with traction-free boundary conditions

$$\sigma_{rr}\left(r_0-\frac{1}{2},\theta\right)=\sigma_{rr}\left(r_0+\frac{1}{2},\theta\right)=\sigma_{r\theta}\left(r_0-\frac{1}{2},\theta\right)=\sigma_{r\theta}\left(r_0+\frac{1}{2},\theta\right)=0 \tag{6}$$

The solution of the eigenvalue problem formulated as Eqs (5) and (6), which gives the exact dispersion equation, can be found in numerous publications.

In what follows, however, we take Eq (3) as a point of departure and notice that, in effect, these equations may be obtained by means of the generalised Galerkin method [8,9]. Indeed, the double integrals are the 'weighted residuals' in differential equations of time-harmonic wave motion, while the single integrals are the 'weighted residuals' in boundary conditions. Therefore, system (3) can be derived with no reference to any variational principle, that is commonly perceived as an essential feature of Galerkin method [8–12]. Furthermore, if the stresses are approximated such that they vanish at the free surfaces $r_0=\pm\frac{1}{2}$, then the single integrals in (3) equal zero and the conventional formulation of Galerkin's method is recovered [12].

We adopt the canonical formulation of any variational method [8–12] and use the same coordinate functions for the unknown displacements' field $u(r,\theta)$, $v(r,\theta)$ and for variations $\delta u(r,\theta)$, $\delta v(r,\theta)$. An approximate solution is sought in the form of expansion of displacements on Legendre polynomials in the radial coordinate specialised for the interval (-½, ½):

$$u(r,\theta)=\sum_{n=1}^{N_u}U_n(\theta)P_{n-1}(r) \tag{7a}$$

$$v(r,\theta)=\sum_{n=1}^{N_v}V_n(\theta)P_{n-1}(r) \tag{7b}$$

These formulas are substituted in (4) so that stresses become:

$$\sigma_{rr}(r,\theta)=\sum_{n=1}^{N_u}\left(\alpha^2U_n(\theta)\frac{dP_{n-1}(r)}{dr}+\left(\alpha^2-2\right)\frac{1}{r}U_n(\theta)P_{n-1}(r)\right)+\sum_{n=1}^{N_v}\left(\alpha^2-2\right)\frac{1}{r}\frac{dV_n(\theta)}{d\theta}P_{n-1}(r)$$
$$\sigma_{\theta\theta}(r,\theta)=\sum_{n=1}^{N_u}\left[\left(\alpha^2-2\right)U_n(\theta)\frac{dP_{n-1}(r)}{dr}+\alpha^2\frac{1}{r}U_n(\theta)P_{n-1}(r)\right]+\sum_{n=1}^{N_v}\alpha^2\frac{1}{r}\frac{dV_n(\theta)}{d\theta}P_{n-1}(r) \tag{8}$$
$$\sigma_{r\theta}(r,\theta)=2\left(\sum_{n=1}^{N_u}\frac{1}{r}\frac{dU_n(\theta)}{d\theta}P_{n-1}(r)+\sum_{n=1}^{N_v}rV_n(\theta)\frac{d}{dr}\left(\frac{P_{n-1}(r)}{r}\right)\right)$$

The variations of displacements are

$$\delta_mu(r,\theta)=\delta U_m(\theta)P_{m-1}(r)$$
$$\delta_mv(r,\theta)=\delta V_m(\theta)P_{m-1}(r) \tag{9}$$

Substitution of (7–9) in (3) and integration in the radial coordinate r gives a system of N_u+N_v differential equations, which may be written in the condensed form

$$\int_{\theta_1}^{\theta_2}\left\{\mathbf{L}_{11m}\left[\sum_{n=1}^{N_u}U_n(\theta)\right]+\mathbf{L}_{12m}\left[\sum_{n=1}^{N_v}V_n(\theta)\right]\right\}\delta U_m(\theta)d\theta=0,\quad m=1,\ldots,N_u \tag{10a}$$

$$\int_{\theta_1}^{\theta_2}\left\{\mathbf{L}_{21m}\left[\sum_{n=1}^{N_u}U_n(\theta)\right]+\mathbf{L}_{22m}\left[\sum_{n=1}^{N_v}V_n(\theta)\right]\right\}\delta V_m(\theta)d\theta=0,\quad m=1,\ldots,N_v \tag{10b}$$

Since the integration limits in θ and variations $\delta U_m(\theta)$ and $\delta V_m(\theta)$ are arbitrary, the expressions in curly brackets should be set to zero:

$$\sum_{n=1}^{N_u}\mathbf{L}_{11m}U_n(\theta)+\sum_{n=1}^{N_v}\mathbf{L}_{12m}V_n(\theta)=0,\quad m=1,\ldots,N_u \tag{11a}$$

$$\sum_{n=1}^{N_u}\mathbf{L}_{21m}U_n(\theta)+\sum_{n=1}^{N_v}\mathbf{L}_{22m}V_n(\theta)=0,\quad m=1,\ldots,N_v \tag{11b}$$

The second-order differential operators $\mathbf{L}_{ijm}$ have an explicit form, because integration of products of Legendre polynomials and their derivatives is done analytically by means of symbolic manipulator Mathematica. The expressions for $\mathbf{L}_{ijm}$ are cumbersome and, therefore, not presented here. By virtue of the generalised Galerkin method, the boundary conditions are accounted for in these operators. It makes them different from the operators, obtained by substitution of series (7–8) in the differential equation (5) and integration over thickness with Legendre polynomials as weight functions. The significance of this feature is highlighted in the analysis of results.

System (11) of the linear ordinary differential equations in θ with constant coefficients describes wave propagation in a curved layer. Its solution has the standard form

$$\begin{aligned}U_n(\theta)&=\widehat{U}_n\exp(\mathrm{i}k\theta)\\V_n(\theta)&=\widehat{V}_n\exp(\mathrm{i}k\theta)\end{aligned} \tag{12}$$

The approximate dispersion equation is obtained by substitution of (12) in Eq (11), cancelling common multiplier $\exp(\mathrm{i}k\theta)$ and equating the determinant of the system of linear algebraic equations in $\widehat{U}_n$and $\widehat{V}_n$ to zero.

This dispersion equation is a polynomial of the order N_u+N_v in k^2. In the limit $r_0\to\infty$ it factorizes to the product of two multipliers, which are the dispersion equations for the symmetric and antisymmetric waves in a straight elastic layer. To model propagation of symmetric waves in a straight layer, even Legendre polynomials should be retained in expansion of the axial displacement (7a) and odd ones in expansion of the radial displacement (7b). To obtain equations for antisymmetric waves, even and odd Legendre polynomials should be swapped.

The branches of dispersion diagram are labelled with the index j, starting from the lowest. For each wavenumber k_j, the shape of displacement field is recovered as

$$\begin{aligned}u_j(r,\theta)&=\sum_{n=1}^{N_u}\widehat{U}_{nj}P_{n-1}(r)\exp(\mathrm{i}k_j\theta)\equiv\widehat{U}_j(r)\exp(\mathrm{i}k_j\theta)\\v_j(r,\theta)&=\sum_{n=1}^{N_v}\widehat{V}_{nj}P_{n-1}(r)\exp(\mathrm{i}k_j\theta)\equiv\widehat{V}_j(r)\exp(\mathrm{i}k_j\theta)\end{aligned} \tag{13}$$

Here $\widehat{U}_j(r)$ and $\widehat{V}_j(r)$ are the profiles of displacements across thickness.

Then stresses are:

$$\sigma_{rrj}(r,\theta)=\left\{\sum_{n=1}^{N_u}\left(\alpha^2\frac{dP_{n-1}(r)}{dr}+\left(\alpha^2-2\right)\frac{1}{r}P_{n-1}(r)\right)\widehat{U}_{nj}+\sum_{n=1}^{N_v}\left(\alpha^2-2\right)\frac{1}{r}\mathrm{i}k_j\widehat{V}_{nj}P_{n-1}(r)\right\}\exp(\mathrm{i}k_j\theta)$$

$$\sigma_{\theta\theta j}(r,\theta)=\left\{\sum_{n=1}^{N_u}\left[\left(\alpha^2-2\right)\tilde{U}_{nj}\frac{dP_{n-1}(r)}{dr}+\alpha^2\frac{1}{r}U_n(\theta)P_{n-1}(r)\right]\widehat{U}_{nj}+\sum_{n=1}^{N_v}\alpha^2\frac{1}{r}\mathrm{i}k_j\widehat{V}_{nj}P_{n-1}(r)\right\}\exp(\mathrm{i}k_j\theta)\tag{14}$$

$$\sigma_{r\theta j}(r,\theta)=2\left\{\sum_{n=1}^{N_u}\frac{1}{r}\mathrm{i}k_j\widehat{U}_{nj}P_{n-1}(r)+\sum_{n=1}^{N_v}r\widehat{V}_{nj}r\frac{d}{dr}\left(\frac{P_{n-1}(r)}{r}\right)\right\}\exp(\mathrm{i}k_j\theta)$$

Expressions in curly brackets present the profiles of stresses $\widehat{\sigma}_{rrj}(r)$, $\widehat{\sigma}_{r\theta j}(r)$ and $\widehat{\sigma}_{\theta\theta j}(r)$ in the radial coordinate for a free wave with the wavenumber k_j. This completes the approximate solution of the free wave propagation problem for an elastic layer of constant curvature and thickness by means of the generalised Galerkin method.

3. Accuracy assessment measures

Formulas (13–14) present non-dimensional displacements and stresses, which are not scaled. It is convenient to normalise displacements to the maximum amplitude of the circumferential one $W_j\equiv\left|\widehat{U}_j(r)\right|_{\max}$ and preserve the same scaling for stresses both in an approximate and an exact solutions. Then the accuracy of solution of the problem of wave propagation in an elastic layer of constant curvature and thickness at any approximation level may directly be assessed by comparison of the field variables formulated as (15) with the exact ones:

$$\tilde{U}_j(r)=W_j^{-1}\sum_{n=1}^{N_u}\widehat{U}_{nj}P_{n-1}(r),\tag{15a}$$

$$\tilde{V}_j(r)=W_j^{-1}\sum_{n=1}^{N_v}\widehat{V}_{nj}P_{n-1}(r),\tag{15b}$$

$$\tilde{\sigma}_{rrj}(r)=W_j^{-1}\left[\sum_{n=1}^{N_u}\left(\alpha^2\frac{dP_{n-1}(r)}{dr}+\left(\alpha^2-2\right)\frac{1}{r}P_{n-1}(r)\right)\widehat{U}_{nj}+\sum_{n=1}^{N_v}\left(\alpha^2-2\right)\frac{1}{r}\mathrm{i}k_j\widehat{V}_{nj}P_{n-1}(r)\right],\tag{15c}$$

$$\tilde{\sigma}_{\theta\theta j}(r)=W_j^{-1}\left[\sum_{n=1}^{N_u}\left[\left(\alpha^2-2\right)\tilde{U}_{nj}\frac{dP_{n-1}(r)}{dr}+\alpha^2\frac{1}{r}U_n(\theta)P_{n-1}(r)\right]\widehat{U}_{nj}+\sum_{n=1}^{N_v}\alpha^2\frac{1}{r}\mathrm{i}k_j\widehat{V}_{nj}P_{n-1}(r)\right],\tag{15d}$$

$$\tilde{\sigma}_{r\theta j}(r)=2W_j^{-1}\left[\sum_{n=1}^{N_u}\frac{1}{r}\mathrm{i}k_j\widehat{U}_{nj}P_{n-1}(r)+\sum_{n=1}^{N_v}r\widehat{V}_{nj}r\frac{d}{dr}\left(\frac{P_{n-1}(r)}{r}\right)\right].\tag{15e}$$

However, the generalised Galerkin method is applicable in a broad class of problems, for which it is difficult, if not at all possible, to obtain an exact solution. Therefore, it is practical to exercise in this example alternative measures of accuracy of approximate solutions, unrelated to the availability of an exact one. For simplicity, hereafter we assume that the equal number of terms is retained in series (15): $N_u=N_v=N$.

Traditionally, the convergence is controlled by comparison of coefficients $\widehat{U}_{nj}$ and $\widehat{V}_{nj}$ obtained at different approximation levels. Such an assessment may be accompanied by two additional measures introduced hereafter. Both these measures are concerned with derivatives of the field variables and, therefore, this convergence criterion is more demanding, than the decay rate of the coefficients in series (15a,b).

The first measure is the magnitudes of scaled tractions at the free surfaces of a layer $\tilde{\sigma}_{rrj}^{(N)}\left(r_{0\pm\frac{1}{2}}\right)$ and $\tilde{\sigma}_{r\theta j}^{(N)}\left(r_{0\pm\frac{1}{2}}\right)$ (N is the number of retained terms), which involve the first derivatives of displacements. These stresses should vanish when $N\to\infty$. The relative accuracy level may be assessed by comparison of these stresses at each approximation level with the normal stresses $\tilde{\sigma}_{\theta\theta j}^{(N)}\left(r_{0\pm\frac{1}{2}}\right)$, which are finite and weakly depend upon N.

The second measure is the radial distribution of scaled residuals, obtained by substitution of formulas (15) in differential equation (5). These functions involve the second derivatives of displacements, and, therefore, converge slower, than both the coefficients in series (13) and the scaled stresses. The residuals equal zero in the exact solution, so that the magnitudes of these functions on their own do not qualify to serve as an accuracy measure. Therefore, a re-scaling should be introduced to

quantify the convergence at different approximation levels. There are five terms in the scaled residual (5a) and four terms in the residual (5b):

$$\tilde{R}_{1j}^{(N)}(r)=\Omega^2\tilde{U}_j^{(N)}(r)+\frac{d\tilde{\sigma}_{rrj}^{(N)}(r)}{dr}+\frac{\mathrm{i}k_j}{r}\tilde{\sigma}_{r\theta j}^{(N)}(r)+\frac{1}{r}\left[\tilde{\sigma}_{rrj}^{(N)}(r)-\tilde{\sigma}_{\theta\theta j}^{(N)}(r)\right], \tag{16a}$$

$$\tilde{R}_{2j}^{(N)}(r)=\Omega^2\tilde{V}_j^{(N)}(r)+\frac{d\tilde{\sigma}_{r\theta j}^{(N)}(r)}{dr}+\frac{\mathrm{i}k_j}{r}\tilde{\sigma}_{\theta\theta j}^{(N)}(r)+\frac{2\tilde{\sigma}_{r\theta j}^{(N)}(r)}{r}. \tag{16b}$$

The new scaling factors $\tilde{W}_{1j}^{(N)}$ and $\tilde{W}_{2j}^{(N)}$ for $\tilde{R}_{1j}^{(N)}(r)$ and $\tilde{R}_{2j}^{(N)}(r)$ are chosen as maximum absolute values of any individual component in (16a) and (16b) attained in the range $r_0-\frac{1}{2}\le r\le r_0+\frac{1}{2}$:

$$R_{1j}^{(N)}(r)=\tilde{R}_{1j}^{(N)}(r)\Big/\tilde{W}_{1j}^{(N)},\quad R_{2j}^{(N)}(r)=\tilde{R}_{2j}^{(N)}(r)\Big/\tilde{W}_{2j}^{(N)}.$$

Then the assessment of accuracy implies comparison of residuals obtained at consecutive approximations, i.e., $R_{1j}^{(N)}(r)$ and $R_{2j}^{(N)}(r)$ with $R_{1j}^{(N+1)}(r)$ and $R_{2j}^{(N+1)}(r)$.

There is one more way to assess the convergence of residuals. If an approximate solution has been obtained with N Legendre polynomials in series (15a,*b*), then the first abandoned terms in displacements are $\Delta_{N+1}\tilde{U}_j(r)=\tilde{U}_{N+1,j}P_N(r)$ and $\Delta_{N+1}\tilde{V}_j(r)=\tilde{V}_{N+1,j}P_N(r)$. To obtain coefficients $\tilde{U}_{N+1,j}$ and $\tilde{V}_{N+1,j}$, the problem with $N+1$ Legendre polynomials retained in series (15a,*b*) should be solved. Substitution of the displacements' increments $\Delta_{N+1}\tilde{U}_j(r)$ and $\Delta_{N+1}\tilde{V}_j(r)$ to (15c,d,e) gives increments to stresses $\Delta_{N+1}\tilde{\sigma}_{rrj}(r)$, $\Delta_{N+1}\tilde{\sigma}_{r\theta j}(r)$ and $\Delta_{N+1}\tilde{\sigma}_{\theta\theta j}(r)$. Then the corrections in differential equation (5) become

$$\Delta_{N+1}\tilde{R}_{1j}(r)=\Omega^2\Delta_{N+1}\tilde{U}_j(r)+\frac{d(\Delta_{N+1}\tilde{\sigma}_{rrj}(r))}{dr}+\frac{\mathrm{i}k_j}{r}\Delta_{N+1}\tilde{\sigma}_{r\theta j}(r)+\frac{1}{r}\left[\Delta_{N+1}\tilde{\sigma}_{rrj}(r)-\Delta_{N+1}\tilde{\sigma}_{\theta\theta j}(r)\right] \tag{17a}$$

$$\Delta_{N+1}\tilde{R}_{2j}(r)=\Omega^2\Delta_{N+1}\tilde{V}_j^{(N)}(r)+\frac{d\left(\Delta_{N+1}\tilde{\sigma}_{r\theta j}(r)\right)}{dr}+\frac{\mathrm{i}k_j}{r}\Delta_{N+1}\tilde{\sigma}_{\theta\theta j}(r)+\frac{2\Delta_{N+1}\tilde{\sigma}_{r\theta j}(r)}{r} \tag{17b}$$

The increments are scaled with the scaling factors $\tilde{W}_{1j}^{(N+1)}$ and $\tilde{W}_{2j}^{(N+1)}$:

$$\Delta_{N+1}R_{1j}(r)=\Delta_{N+1}\tilde{R}_{1j}(r)\Big/\tilde{W}_{1j}^{(N+1)},\quad \Delta_{N+1}R_{2j}(r)=\Delta_{N+1}\tilde{R}_{2j}(r)\Big/\tilde{W}_{2j}^{(N+1)}.$$

These functions should be compared with the residuals (16) calculated with N Legendre polynomials in series (15). Closeness of functions (16) and (17) illustrates convergence.

It is also possible to roughly assess values of $\tilde{U}_{N+1,j}$, $\tilde{V}_{N+1,j}$ without solving the problem with $N+1$ Legendre polynomials in series (15). Then these amplitudes are considered as unknowns to be found from equations $\Delta_{N+1}R_{mj}(r)=R_{mj}^{(N)}(r)$, $m=1,2$, which have to be converted to an algebraic form by averaging in radial coordinate.

4. Dispersion diagrams

The exact formulation of dispersion equation for an elastic layer of the constant curvature (see Refs. [3,13]) involves Bessel functions with, in general, complex-valued wavenumbers as indices and frequency parameter as an argument. It presents serious computational difficulties to find all wavenumbers and customarily the analysis of roots of dispersion equation is confined only to purely real ones, which characterise propagating waves.

The solution method outlined in the previous section delivers at any approximation level a polynomial dispersion equation both in wavenumber and frequency parameter, rather than a transcendental one, with no limitations on frequency and wavenumber ranges. Therefore, all roots of the polynomial dispersion equation are found at once very easily. In contrast to the conventional low-frequency approximation of the exact dispersion equation, in which logarithmic terms containing the frequency parameter emerge, this polynomial contains a single logarithmic parameter $\ln\left(1+\frac{2}{2r_0-1}\right)$, which characterises the geometry of a curved layer.

It is a straightforward matter to see that adding a term in series (15) brings an additional branch to the dispersion diagram. Since the determinant is not diagonal, this extension of series affects location of all branches found at the previous level of approximation. However, the cut-on frequencies of low-order branches converge to their exact values very rapidly, so that, for instance, the location of the second branch for moderately large wavenumbers remains virtually fixed as soon as $N>1$.

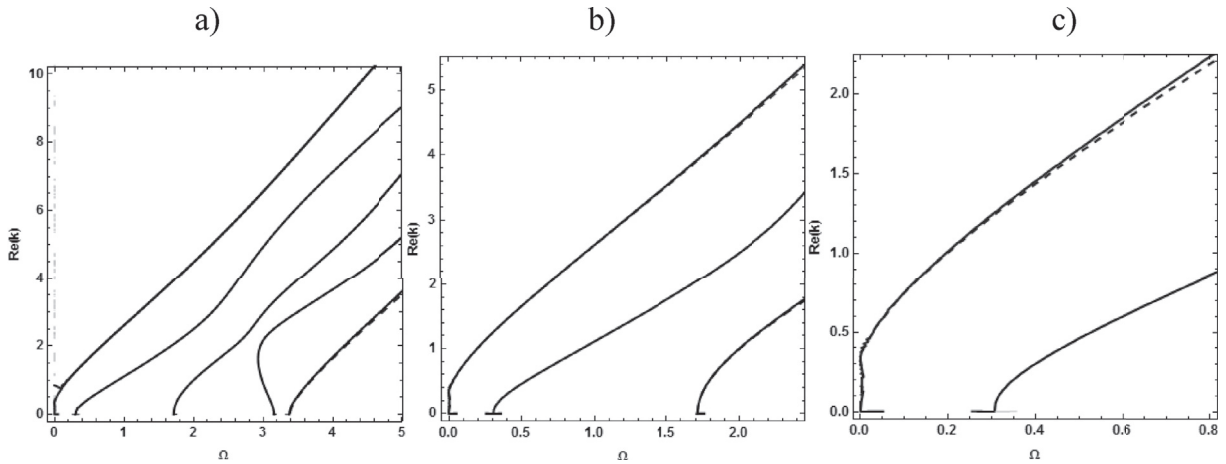

Fig. 1. Approximate solutions (a) $N = 6$ (dashed curves), (b) $N = 4$ (dashed curves) and (c) $N = 3$ (dashed curves) compared with exact dispersion curves (solid curves); $r_0 = 3$.

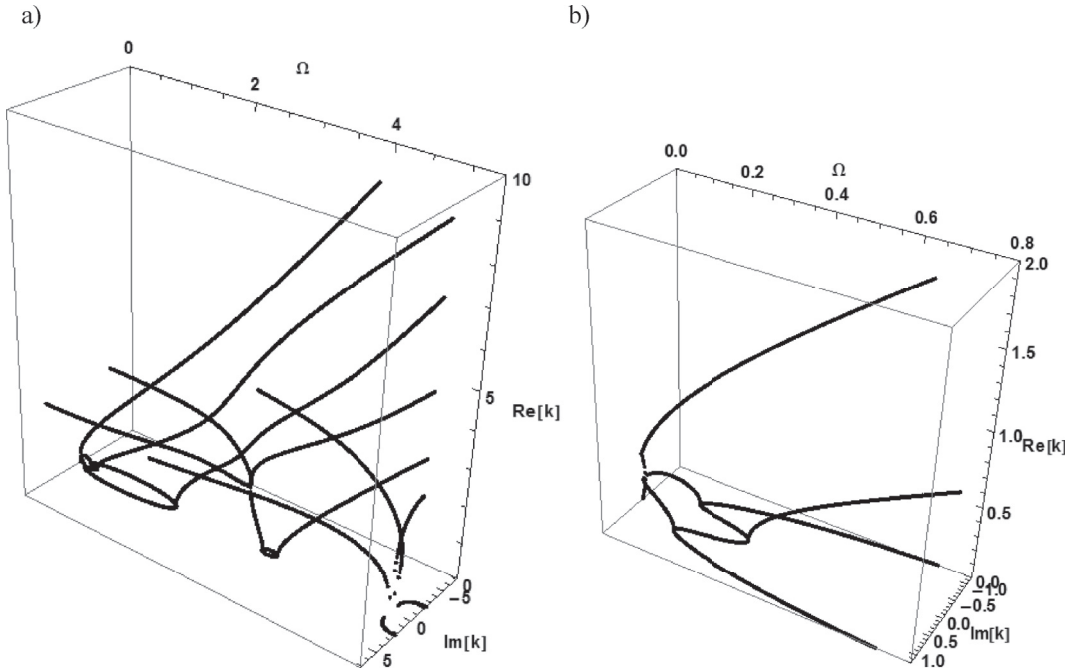

Fig. 2. 3D Dispersion diagrams (a) from Fig. 1a, $N = 6$ and (b) from Fig. 1c, $N = 3$.

We begin with the accuracy assessment of solutions of dispersion equations for several truncation levels in series (15). In Fig. 1, dispersion diagram obtained in the exact problem formulation (see Refs. [3,13]) is compared with its counterpart with (a) $N = 6$, (b) $N = 4$ and (c) $N = 3$ for $r_0 = 3$. The comparison is restricted only to purely real wavenumbers. In each window, there is an excellent agreement between approximate and exact solutions. To enlarge the size of a window, where an approximate solution is accurate, more terms should be kept in expansions (15).

If the purely imaginary and complex-valued wavenumbers should also be shown, then it is more convenient to present the dispersion diagram in 3D as done in Fig. 2 for the same curvature parameter, $r_0 = 3$, the same frequency ranges and the same range of $\mathrm{Re}[k]$. The graphs in Fig. 2 are plotted after $N = 6$ (a) and $N = 3$ (b) approximations in the frequency ranges, where these solutions are undistinguishable from their exact counterparts. It is profoundly cheaper to obtain the approximate solution, than to solve the exact dispersion equation. Graphs in both Figures are plotted only for $\mathrm{Re}[k] \geq 0$ due to the symmetry of dispersion diagrams with respect to the plane $\mathrm{Re}[k] = 0$.

Notably, the generalised Galerkin method strongly improves accuracy of the low-order approximations as compared with the simplified approach used in Ref. [6] for analysis of elastic waves in a straight layer. There is no need to tune the cut-on frequencies in a reduced model to their exact values by means of inertia-correction coefficients. For example, the cut-on frequency of the second branch found in $N = 3$ approximation, $\Omega_{cut-on,2} = 0.305009$ differs in 0.01% from its exact value, $\Omega_{cut-on,2} = 0.304987$. For the $N = 6$ approximation, the first four cut-on frequencies attain their exact values. The fifth cut-on frequency, $\Omega_{cut-on,5} = 3.38873$ differs only in 0.3% from its exact value, $\Omega_{cut-on,5} = 3.3766$.

5. The field shapes and error estimates

The dispersion diagrams present global characteristics of free waves. To assess the accuracy of approximations in fine details, the shapes of field variables (displacements and stresses) should be examined in the representative zones in dispersion diagrams. In what follows in this section, the curvature parameter is set as $r_0 = 3$.

5.1. The strong coupling zone

We begin with the inspection of displacements, stresses and error estimates in the low-frequency 'strong coupling zone', shown in the down left corners of Fig. 1 and zoomed in Fig. 3. The dispersion relation in this region has been thoroughly analysed in Ref. [13], Section 4(a), where an elementary polynomial dispersion equation of the third order in k^2 has been rigorously derived and shown to be asymptotically consistent with the exact theory in the low frequency – small wavenumber limit. The main motivation to re-visit this case here is to study the distribution of displacements and stresses in view of kinematic assumptions adopted in the elementary beam theory.

As seen from Fig. 3, the $N = 2$ approximation is not sufficiently accurate, so that the dispersion equation with $N = 3$ is considered hereafter. This is a polynomial of the sixth order in k^2 and the three dispersion curves in Fig. 3 are virtually undistinguishable from those predicted by the exact theory.

The magnitude of wavenumber at $\Omega = 0$ at any approximation level matches its exact value, $k = \frac{1}{r_0}$, whereas the tangent to the dispersion curve at the origin of coordinate, which has the exact magnitude oftan $\Psi = \frac{\sqrt{12}(1-\nu)}{\sqrt{1-2\nu}} r_0$ (ν is the Poisson ratio) differs from this formula with the correction factor, which weakly depends upon r_0. The explicit formula for this factor when $N = 3$ is cumbersome and it contains the logarithmic term $\ln\left(1 + \frac{2}{2r_0-1}\right)$. The same holds true for coordinates of the point, where the group velocity is zero. In exact form, these coordinates are independent upon r_0: $\Omega_G = \sqrt{\frac{71-17\sqrt{17}}{8}}, k_G = \sqrt{\frac{\sqrt{17}-3}{4}}$. As seen from Fig. 3, location of this point is predicted by the $N = 3$ Galerkin approximation with high accuracy, but the explicit formulas for its coordinates are also cumbersome and feature the same logarithmic term $\ln\left(1 + \frac{2}{2r_0-1}\right)$.

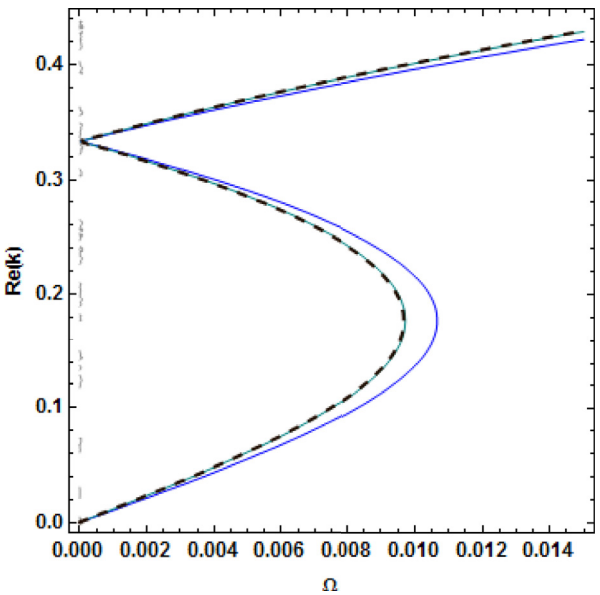

Fig. 3. Dispersion diagram in the strong coupling zone: the $N = 3$ approximation and the exact solution (both blue) versus the $N = 2$ approximation (dashed).

The polynomial dispersion equation obtained by generalised Galerkin method, unlike Eq. (4.1) in Ref. [13], does not asymptotically agree with the exact solution and it is of the sixth order, rather than only of the third order in k^2. However, the dispersion equation (4.1) in Ref. [13] is not directly linked to the field variables. Therefore, a considerable amount of extra work, similar to that for anti-symmetric waves in a straight layer reported in Ref. [7], needs to be done in the framework of the model used in Ref. [13] to explore distribution of the field variables. Such an analysis of distribution of displacements and stresses across the thickness and the accuracy assessment of approximations obtained by means of the generalised Galerkin method are performed hereafter and we are of opinion that these both constitute aspects of novelty of the paper.

As seen in Fig. 3, there are three branches in dispersion diagram, which describe propagating waves at the frequency $\Omega = 0.002$. For the first (lowest) branch, the wavenumber is $k_1 = 0.0235$. In Fig. 4, displacements (a) and stresses (b), scaled as explained in Section 2, are shown. Distribution of the axial displacement $\tilde{U}_1(r)$ across the thickness is presented in green, and distribution of the radial displacement $\tilde{V}_1(r)$ is in red. Normal radial stresses $\tilde{\sigma}_{rr1}(r)$ are plotted in red, normal axial stresses $\tilde{\sigma}_{\theta\theta 1}(r)$ are in green, and shear stresses $\tilde{\sigma}_{r\theta 1}(r)$ are in blue. These colours are used in the same way in all Figures hereafter.

As seen from Fig. 4, accurate prediction of location of the dispersion curve entails almost equally accurate presentation of displacements and stresses. Maximal discrepancies in the approximation $N = 3$ are in the radial normal stresses at the traction-free surfaces. However, these should be compared with the axial stresses $\tilde{\sigma}_{\theta\theta 1}(r)$, which do not turn to zero. The ratio at this level of approximation is $\frac{\tilde{\sigma}_{rr1}\left(r_{0\pm\frac{1}{2}}\right)}{\tilde{\sigma}_{\theta\theta 1}\left(r_{0\pm\frac{1}{2}}\right)} \approx 0.12$. There is a phase shift of $\frac{\pi}{2}$ between displacements, and the radial displacement $\tilde{V}_1(r)$ is dominant. It is linearly dependent upon coordinate and, due to the curvature, is larger at the outer surface of the layer, than at the inner layer. The axial displacement $\tilde{U}_1(r)$ is uniformly distributed across thickness. Therefore, the 'plane cross-section' kinematics is valid. The distribution of bending stresses $\tilde{\sigma}_{\theta\theta 1}(r)$ follows the classical theory of bending of curved beams. The normal stresses are in phase with each other, whereas the shear stresses are shifted in $\frac{\pi}{2}$ to them.

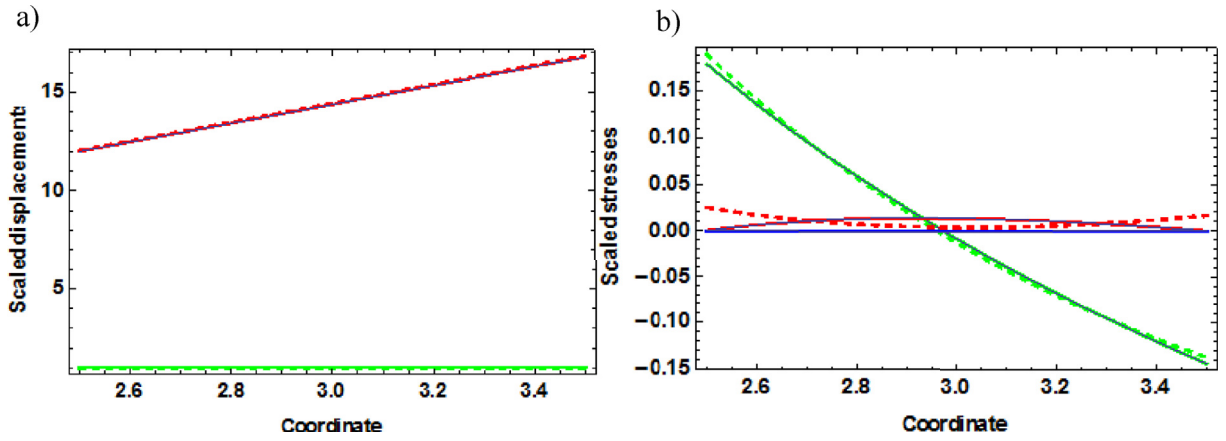

Fig. 4. Scaled displacements (a) and stresses (b), $\Omega = 0.002$, $k_1 = 0.0235$. Dashed lines: approximation $N = 3$, solid lines: approximation $N = 6$; thin lines: exact solution.

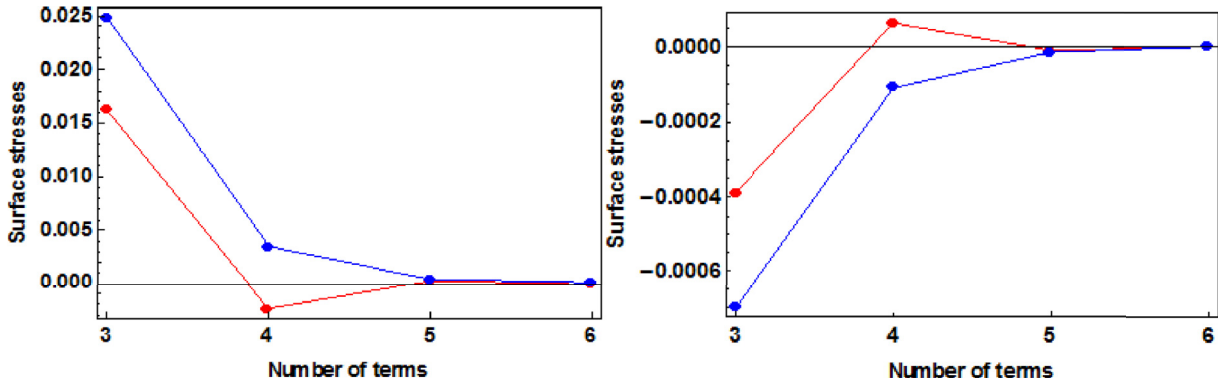

Fig. 5. Convergence to zero of tractions at free surfaces, $\Omega = 0.002$, $k_1 = 0.0235$: a) $\tilde{\sigma}_{rr1}(r)$, b) $\tilde{\sigma}_{r\theta 1}(r)$. Red curves for $r = \frac{7}{2}$ (outer surface), blue curves for $r = \frac{5}{2}$ (inner surface).

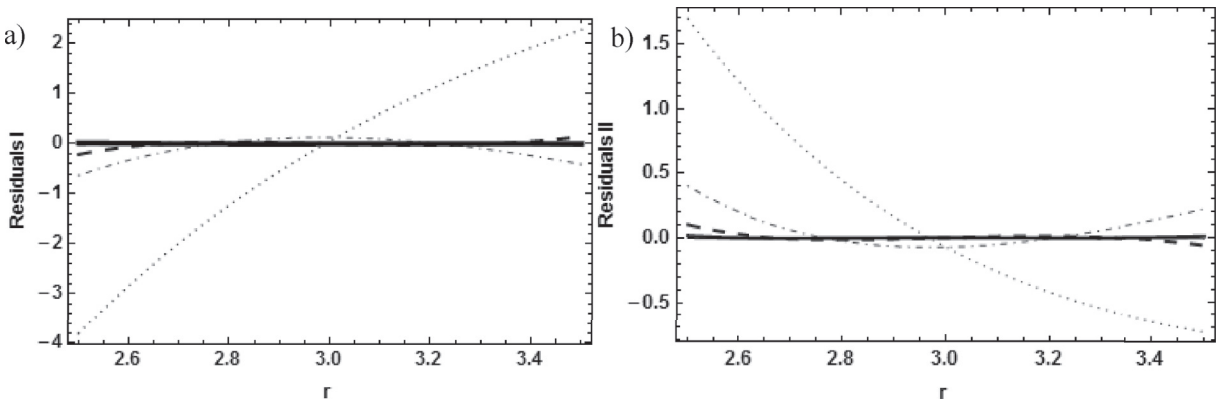

Fig. 6. Residuals $R_{11}^{(N)}(r)$ (a), $R_{21}^{(N)}(r)$ (b), $\Omega = 0.002$, $k_1 = 0.0235$: $N = 3$(Dotted), $N = 4$(dashed-dotted), $N = 5$(dashed), $N = 6$(solid).

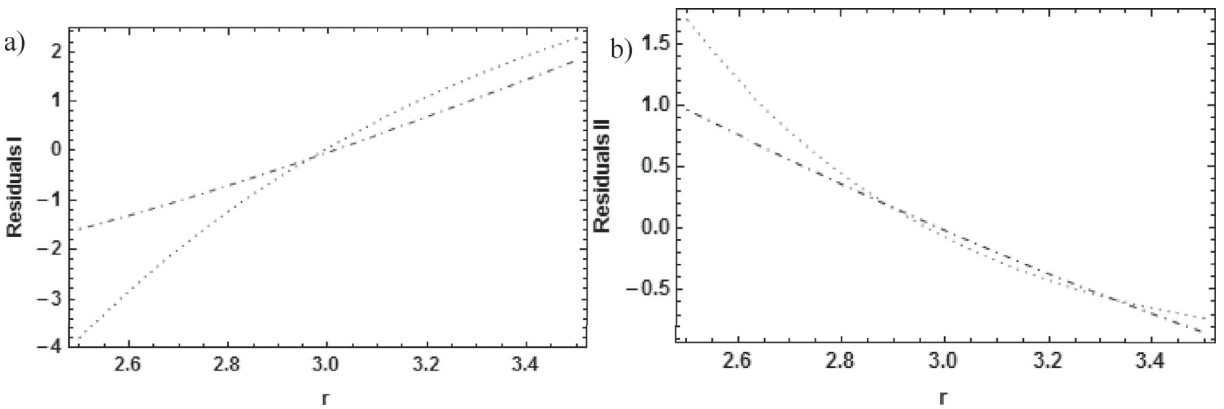

Fig. 7. The functions $R_{11}^{(3)}(r)$, $\Delta_4 R_{11}(r)$ (a) and $R_{21}^{(3)}(r)$, $\Delta_4 R_{21}(r)$ (b).

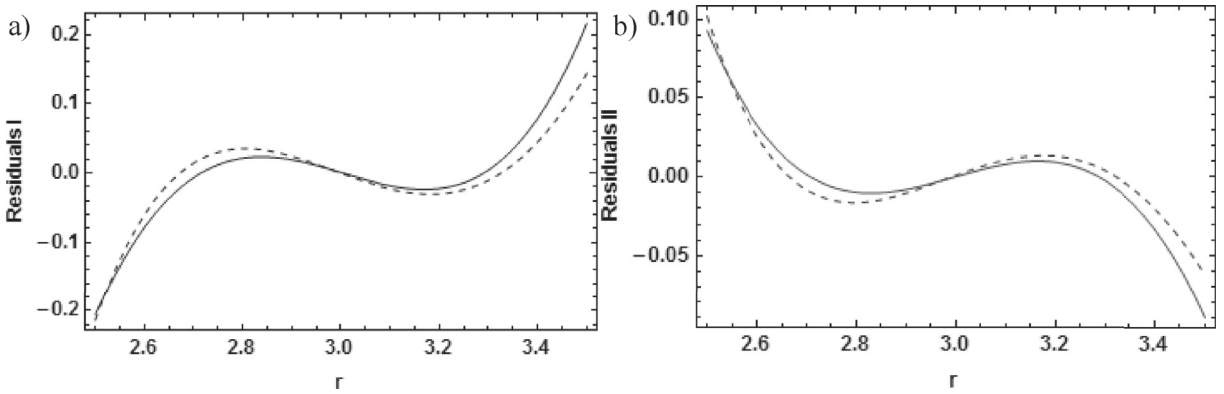

Fig. 8. The functions $R_{11}^{(5)}(r)$, $\Delta_6 R_{11}(r)$ (a) and $R_{11}^{(5)}(r)$, $\Delta_6 R_{21}(r)$ (b).

In Fig. 5, the tractions at free surfaces, $\tilde{\sigma}_{rr1}\left(r_{0\pm\frac{1}{2}}\right)$ and $\tilde{\sigma}_{r\theta 1}\left(r_{0\pm\frac{1}{2}}\right)$ are presented versus number of terms N in series (15) As seen, already with five terms in each series, the discrepancy in formulation of boundary conditions at free surfaces virtually vanishes.

One more error estimate is the residuals $R_{11}^{(N)}(r)$ and $R_{21}^{(N)}(r)$, see formulas (16). This measure accounts for derivatives of stresses, and, therefore, the second derivatives of displacements, approximated with Legendre polynomials. As seen in Fig. 6, the convergence is rather fast. Another important observation is that at each level of approximation a set of grid points exists,

where the approximate solution satisfy the differential equations of elasto-dynamics exactly. The number of these grid points is determined by the number of zeros of functions $\Delta_{N+1}R_{mj}(r)$, $m = 1, 2$ or, which is the same, functions $R^{(N)}_{mj}(r)$, $m = 1, 2$ along the length of a layer $r_0 - \frac{1}{2} \le r \le r_0 + \frac{1}{2}$. It is easy to show that this number is $N - 2$.

As already discussed, both the amplitude and the shape of residual functions provide useful information regarding contributions of the neglected terms. Therefore, we explore this issue in more detail. In Fig. 7, dotted curves represent the functions $R^{(3)}_{11}(r)$ and $R^{(3)}_{21}(r)$, while the dashed-dotted curves are plotted after the functions $\Delta_4 R_{11}(r)$ and $\Delta_4 R_{21}(r)$. As seen, the dominant contribution to the residuals indeed comes from the fourth terms in expansions (15a,b).

In Fig. 8, the residuals $R^{(5)}_{11}(r)$ and $R^{(5)}_{21}(r)$ (dashed curves) are compared with $\Delta_6 R_{11}(r)$ and $\Delta_6 R_{21}(r)$ (solid curves). The magnitudes of residuals in the case illustrated in Fig. 7 are one order of magnitude larger, than in this one. In both cases, however, there is a perfect match between the shapes (number of grid points) of these functions. It suggests that contribution of all remaining neglected terms to stresses and their derivatives is less than the first neglected one, i.e., solution is converged with the known tolerance.

The second wave at $\Omega = 0.002$ has the wavenumber $k_2 = 0.316$ It is characterised with the displacements and stresses shown in Fig. 9.

The third wave at $\Omega = 0.002$ with $k_3 = 0.349$ is characterised in the same way in Fig. 10.

These two waves may be referred to as the flexural ones, which perfectly follow the 'plane cross-section' kinematics. The second one can be called anomalous, because it features opposite directions of phase and group velocities, $c_{phase} \cdot c_{group} < 0$, whereas the third wave is the conventional flexural wave, which, as well known [1], transforms in a straight layer to the Rayleigh wave at high frequencies. There is virtually no difference in spatial characteristics of these waves. The assessment of accuracy replicates the one conducted for the first wave and, therefore, not presented here.

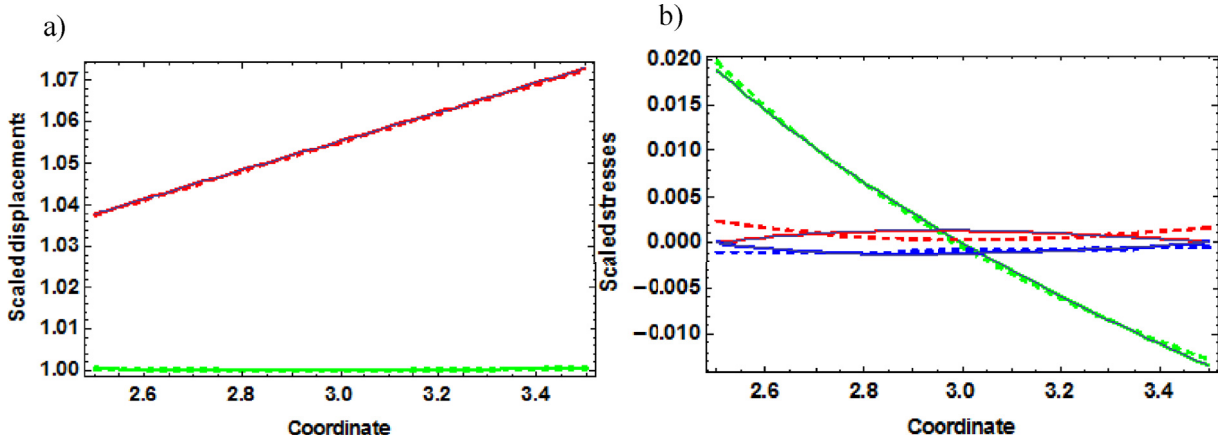

Fig. 9. Scaled displacements (a) and stresses (b), $\Omega = 0.002$, $k_2 = 0.316$. Dashed lines: approximation $N = 3$, solid lines: approximation $N = 6$; thin lines: exact solution.

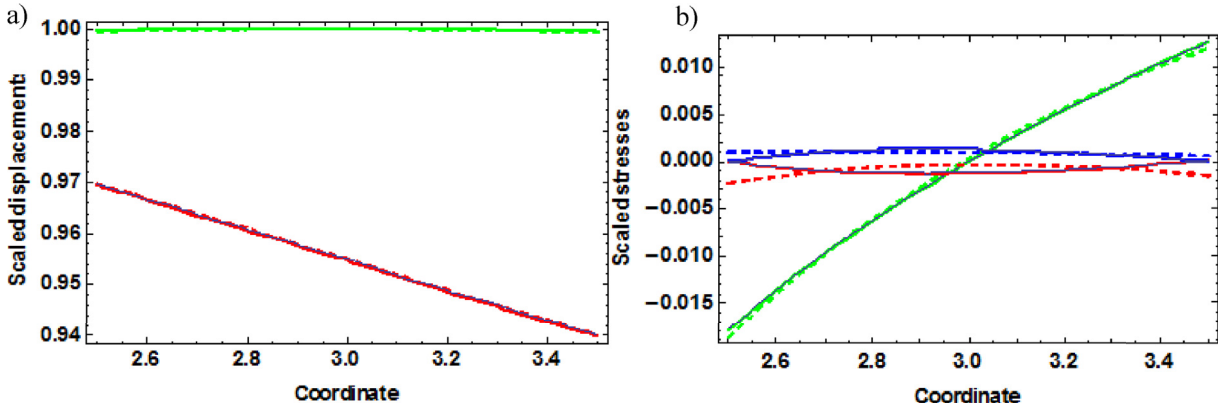

Fig. 10. Scaled displacements (a) and stresses (b), $\Omega = 0.002$, $k_3 = 0.349$. Dashed lines: approximation $N = 3$, solid lines: approximation $N = 6$; thin lines: exact solution.

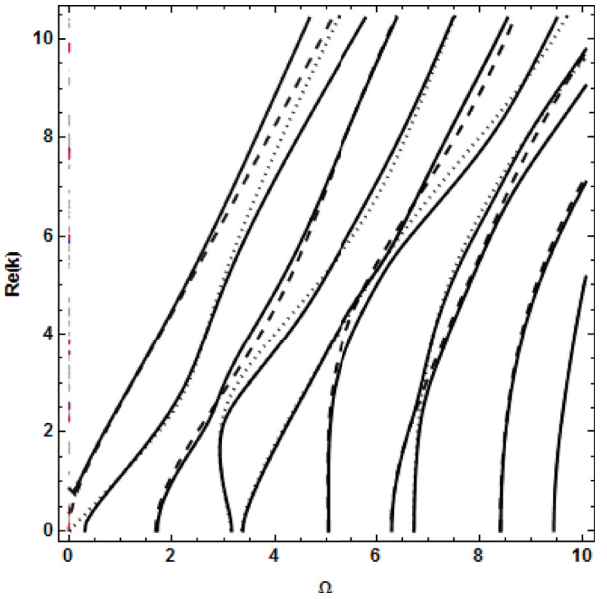

Fig. 11. Dispersion diagram (real-valued wavenumbers) for a straight layer (dashed – anti-symmetric waves, dotted – symmetric waves) and for a curved layer with $r_0 = 3$ (solid).

On balance, we conclude that the $N = 3$ approximation by means of the generalised Galerkin method is highly accurate in prediction of location of dispersion curves and distribution of the field variables in the strong coupling zone – although the dispersion relation is not asymptotically consistent with its exact form.

5.2. The 'Rayleigh branch'

In Fig. 11, the dashed curves present branches of dispersion diagram for anti-symmetric waves in a straight layer of constant thickness, the dotted curves are plotted for symmetric waves in this layer and the solid curves display the dispersion diagram for a curved layer with $r_0 = 3$. All dispersion curves are plotted after numerical solutions of the problems in their exact formulation. As seen, the canonical dispersion diagrams for the Rayleigh-Lamb problem [1,2] are rather similar to the dispersion diagram for a curved layer, even if the curvature is large. The main exception is the down left corner of the diagram, where strong coupling takes place. This zone, zoomed in Fig. 3, is not seen in the range used in Fig. 11. Elsewhere in a broad frequency/wavenumber range the branches for a curved layer exhibit veering in the zones of their intersection for a straight layer.

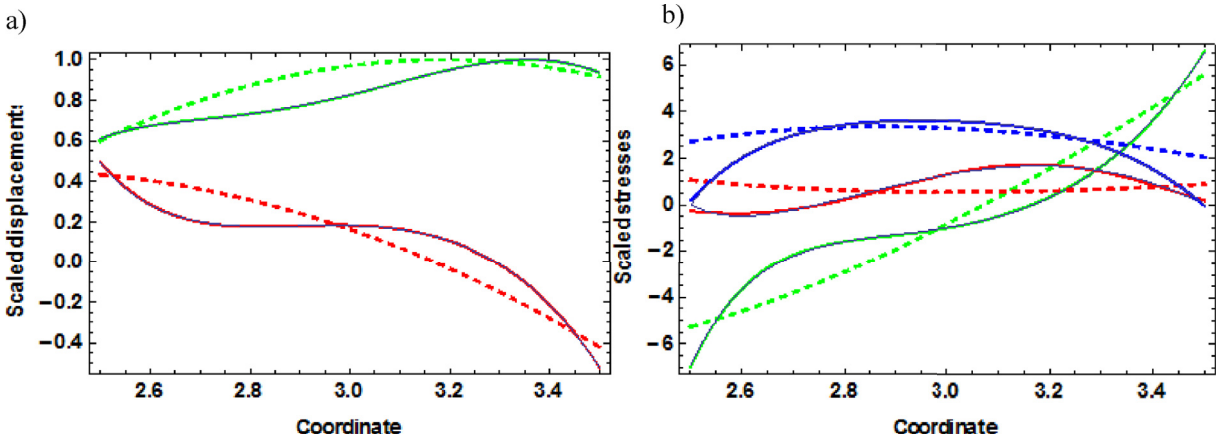

Fig. 12. Scaled displacements (a) and stresses (b), $\Omega = 2.0$, $k_R = 4.494$, Rayleigh branch. Dashed lines: approximation$N = 3$, solid lines: approximation $N = 6$; thin lines: exact solution.

The upper branch in the dispersion diagram shown in Fig. 11 is known as the 'Rayleigh branch' in analysis of propagation of anti-symmetric waves in a straight layer [1,2]. In the low frequency limit, the wave described by this branch is the flexural wave modelled by the classical Bernoulli-Euler beam theory. As the frequency grows, its cross-sectional profile transforms to two surface waves, similar to the Rayleigh wave at the surface of an elastic half-space. Here we study evolution of this wave in a curved layer with $r_0 = 3$.

The field variables and error measures for the flexural propagating waves at a very low frequency $\Omega = 0.002$ are shown in Figs. 9 and 10 and discussed in the previous subsection. Advancing to the frequency $\Omega = 0.02$ means that the strong coupling region is left, and there is only one propagating wave with $k_R = 0.456$. The same holds true for the frequency parameter $\Omega = 0.2$, see Fig. 1c, where this wave is characterised by the wavenumber $k_R = 1.014$. However, despite the 10- and 100 times differences in Ω, the profiles of displacements and stresses in both cases remain the same as at $\Omega = 0.002$, $k_R = k_3 = 0.349$. The radial displacement is linearly distributed, and it fits the 'plane cross-section' kinematics. At $\Omega = 0.02$, it varies from 0.83 at the inner surfaces to 0.63 at the outer surface, and at $\Omega = 0.2$ it varies from 0.7 to almost zero. The shapes of stress distributions at $\Omega = 0.02$ and $\Omega = 0.2$ are the same as shown in Fig. 10, but their magnitudes are much larger. Both at $\Omega = 0.02$ and $\Omega = 0.2$ the three-term approximation of displacement field provides sufficient accuracy, and the six-term one perfectly matches the exact solution.

If the frequency is even higher, $\Omega = 2.0$, then the shape of displacements and stresses at the 'Rayleigh branch' markedly departs from the elementary theory and the three-term model does not capture these fields accurately as seen in Fig. 12. It should be noted that at $\Omega = 2.0$ this model predicts the wavenumber as $k_R = 4.320$, whereas the exact value (also obtained in the six-term model) is $k_R = 4.494$. The radial displacements have opposite signs at the inner and outer surface of a layer, and shear stresses at the middle of the layer are only two times less than the axial normal ones.

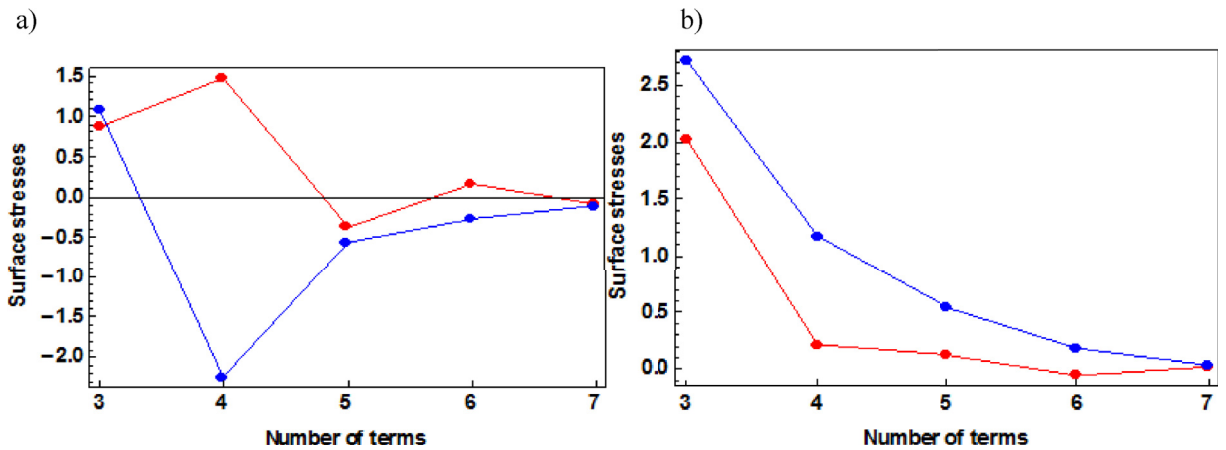

Fig. 13. Convergence to zero of tractions at free surfaces$\Omega = 2.0$, $k_R = 4.494$, Rayleigh branch $\tilde{\sigma}_{rr3}(r)$ (a), $\tilde{\sigma}_{r\theta 3}(r)$ (b). Red curves $r = \frac{7}{2}$(outer surface), blue curves $r = \frac{5}{2}$(inner surface).

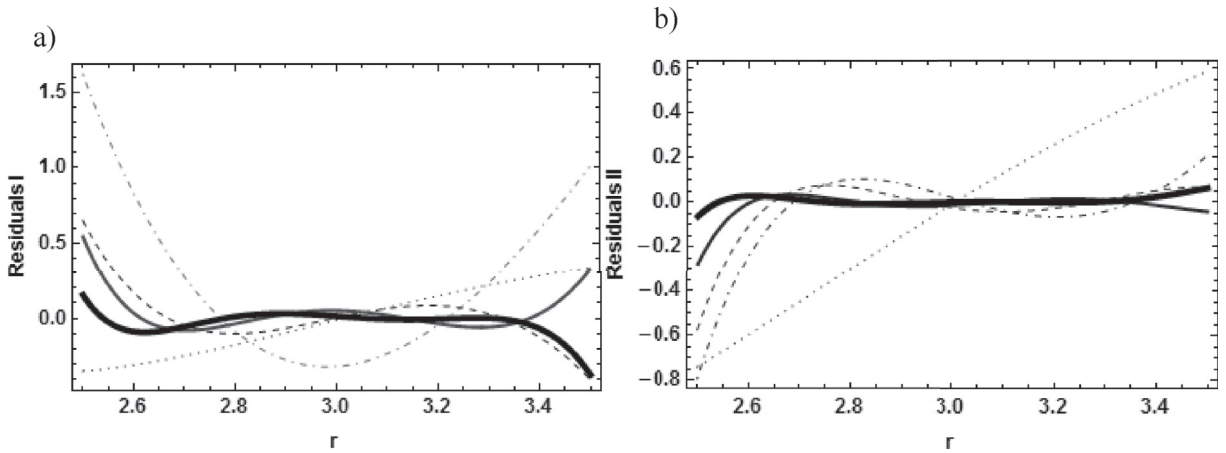

Fig. 14. Residuals $R_{1R}^{(N)}(r)$ (a), $R_{2R}^{(N)}(r)$ (b), $\Omega = 2.0$, $k_R = 4.494$, Rayleigh branch: $N = 3$(dotted), $N = 4$(dashed-dotted), $N = 5$(dashed), $N = 6$(solid), $N = 7$(bold solid).

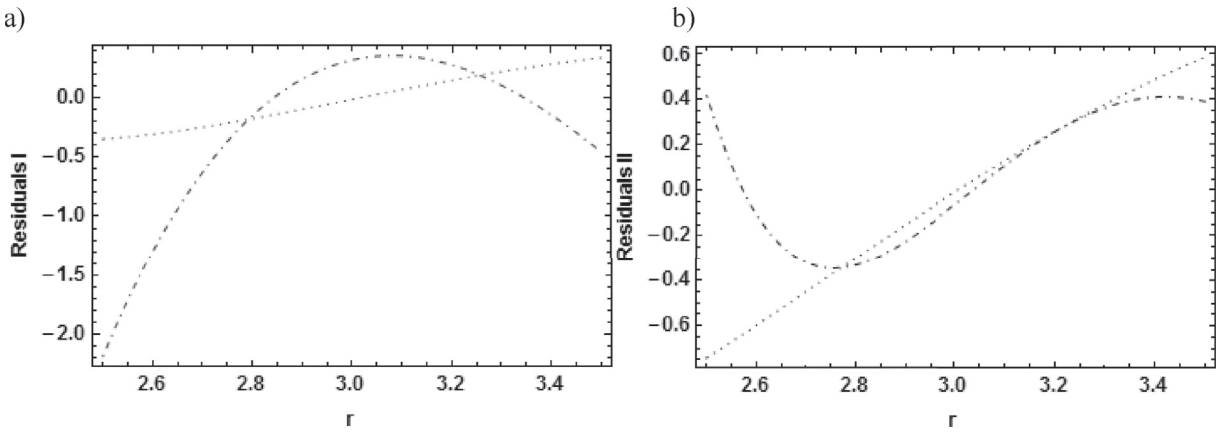

Fig. 15. The functions $R_{1R}^{(3)}(r)$, $\Delta_4 R_{1R}(r)$ (a) and $R_{2R}^{(3)}(r)$, $\Delta_4 R_{2R}(r)$ (b) $\Omega = 2.0$, $k_R = 4.494$, Rayleigh branch.

The convergence of surface stresses is illustrated in Fig. 13, and this study is extended to the $N = 7$ approximation. The residuals $R_{1R}^{(N)}(r)$ and $R_{2R}^{(N)}(r)$ are plotted in Fig. 14.

In contrast to Figs. 7–8, there is the non-uniform convergence of accuracy measures. Specifically, the results obtained with $N = 3$ seem to be more accurate than with $N = 4$ (Figs. 13a and 14a). To analyse the difference, the graphs in Figs. 15 and 16 should be compared with each other.

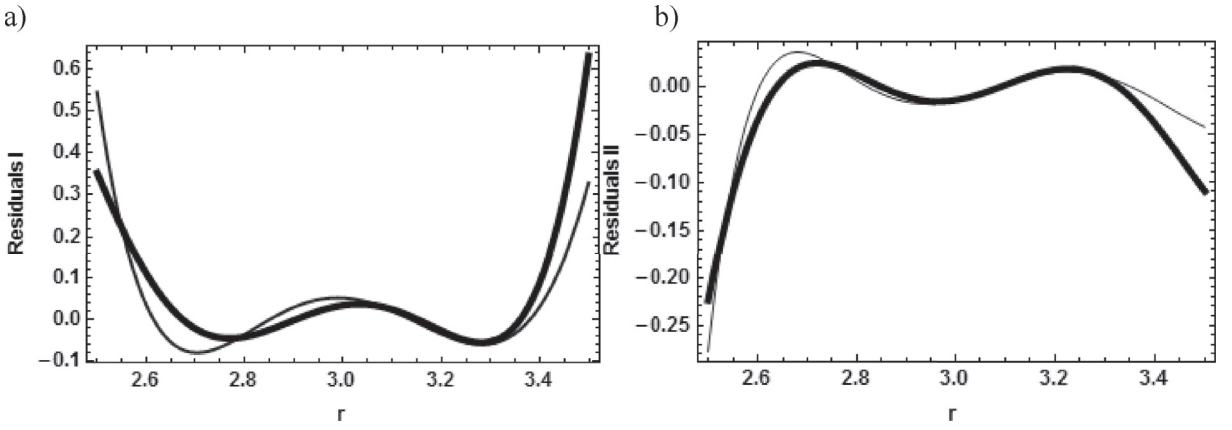

Fig. 16. The functions $R_{1R}^{(6)}(r)$, $\Delta_7 R_{1R}(r)$ (a) and $R_{1R}^{(6)}(r)$, $\Delta_7 R_{2R}(r)$ (b) $\Omega = 2.0$, $k_R = 4.494$, Rayleigh branch.

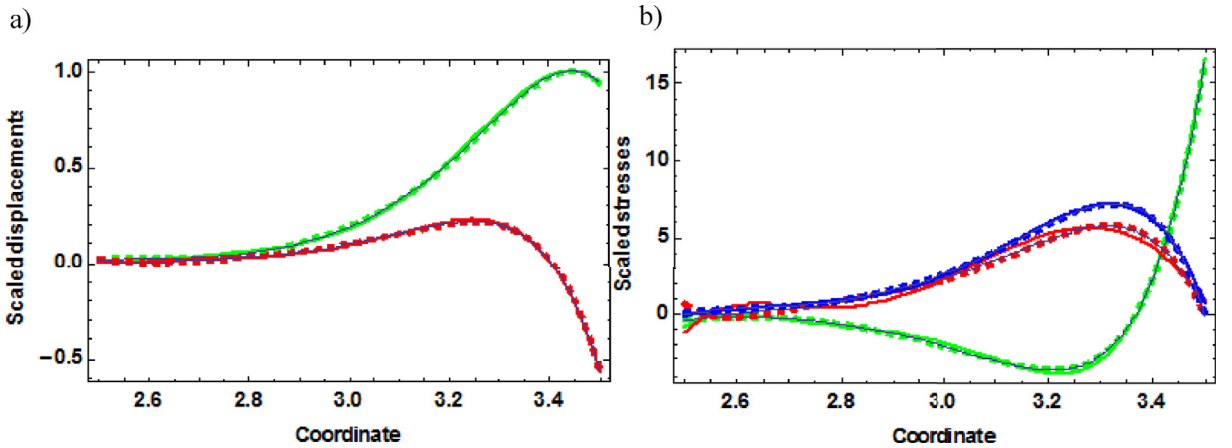

Fig. 17. Scaled displacements (a) and stresses (b), $\Omega = 5.0$, $k_R = 11.193$, Rayleigh branch Solid/dashed lines: approximations $N = 6/N = 7$, thin lines: exact solution.

The functions $R_{1R}^{(3)}(r)$, $R_{2R}^{(3)}(r)$ (dotted curves) are compared with the functions $\Delta_4 R_{1R}(r)$ and $\Delta_4 R_{2R}(r)$ (dashed-dotted curves) in Fig. 15. In contrast to the similar graphs in Fig. 7, the curves are much different, so that the dominant contribution to the correct shape does not come from the fourth terms in (15). Therefore, the $N = 3$ is not converged. In Fig. 16, the functions $R_{1R}^{(6)}(r)$, $R_{2R}^{(6)}(r)$ (solid curves) are compared with the functions $\Delta_7 R_{1R}(r)$ and $\Delta_7 R_{2R}(r)$ (bold solid curves). At this approximation level, there is a good agreement between the shapes of these curves, and this indicates that the solution has converged.

At frequency $\Omega = 5.0$, the three-term model fails completely, so that only exact results, results obtained with $N = 6$ and results obtained with $N = 7$ are shown in Fig. 17. There is an excellent agreement between them regarding the wavenumber, $k_R = 11.193$, displacements and stresses.

The distribution of displacements now resembles the Rayleigh wave travelling along the outer surface of a curved layer. The amplitudes of displacements and axial normal stresses $\sigma_{\theta\theta}$ decay at the inner surface. These diagrams may be compared with the similar ones in Ref. [7]: Figs. 2c and 3c for the first anti-symmetric wave in a straight layer at approximately the same frequency. In these Figures, V, T_{xy} and U, T_{yy} are symmetric/anti-symmetric functions of the coordinate Y counted from the symmetry axis of a layer. Their pattern is similar to what is shown in Fig. 17. The main difference, however, is that surface waves emerge at the both sides of a straight layer (the range is $0 \le Y \le \frac{1}{2}$ in Ref. [7], so that the same wave exists at $-\frac{1}{2} \le Y \le 0$) and only at the outer side of a curved layer. This result is hardly surprising because it perfectly matches the canonical 'whispering gallery' effect described by Lord Rayleigh [14].

The residuals $R_{1R}^{(N)}(r)$ and $R_{2R}^{(N)}(r)$ are plotted in Fig. 18.

In Fig. 19, the functions $R_{1R}^{(6)}(r)$, $R_{2R}^{(6)}(r)$ (solid curves) are compared with the functions $\Delta_7 R_{1R}(r)$ and $\Delta_7 R_{2R}(r)$ (bold solid curves). Similarly to the case illustrated in Fig. 16, the closeness between them suggests that the solution is converged.

Finally, we present the field variables for the 'Rayleigh branch' at the frequency $\Omega = 10.0$ in Fig. 20. First of all, it should be observed that this frequency lies outside the validity box of the six-term model. The exact magnitude of wavenumber for this

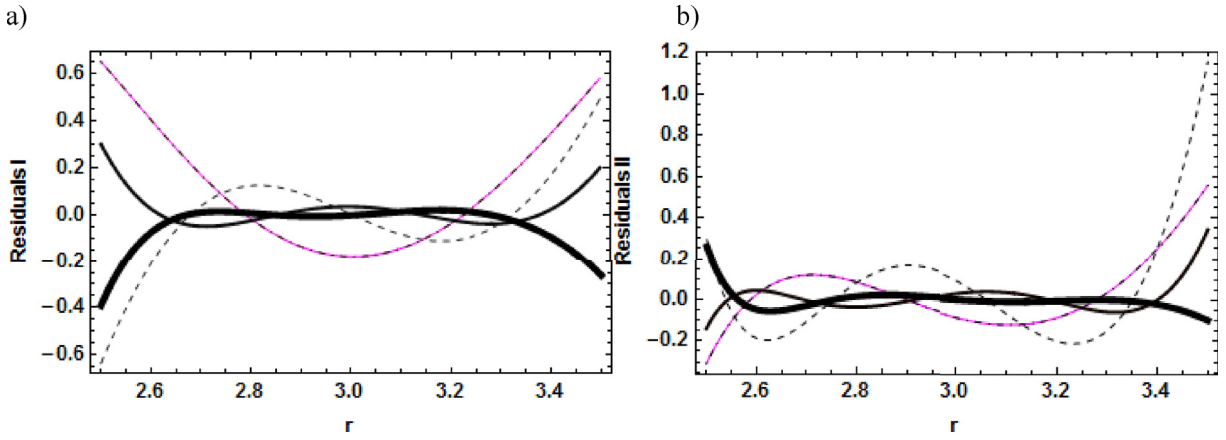

Fig. 18. Residuals $R_{1R}^{(N)}(r)$ (a), $R_{2R}^{(N)}(r)$ (b), $\Omega = 5.0$, $k_R = 11.193$, Rayleigh branch: $N = 4$(magenta), $N = 5$(dashed), $N = 6$(solid), $N = 7$(bold solid).

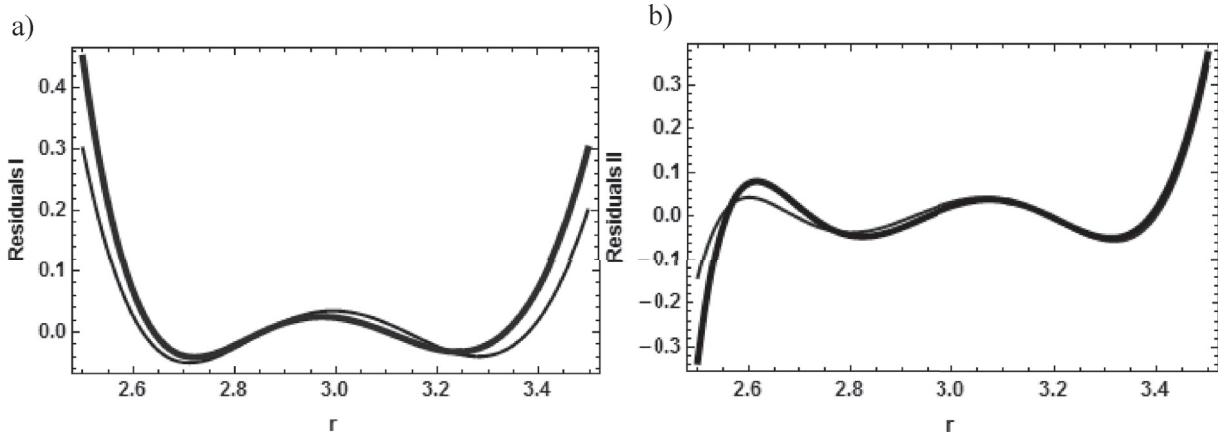

Fig. 19. The functions $R_{1R}^{(6)}(r)$, $\Delta_7 R_{1R}(r)$ (a) and $R_{1R}^{(6)}(r)$, $\Delta_7 R_{2R}(r)$ (b) $\Omega = 5.0$, $k_R = 11.193$, Rayleigh branch.

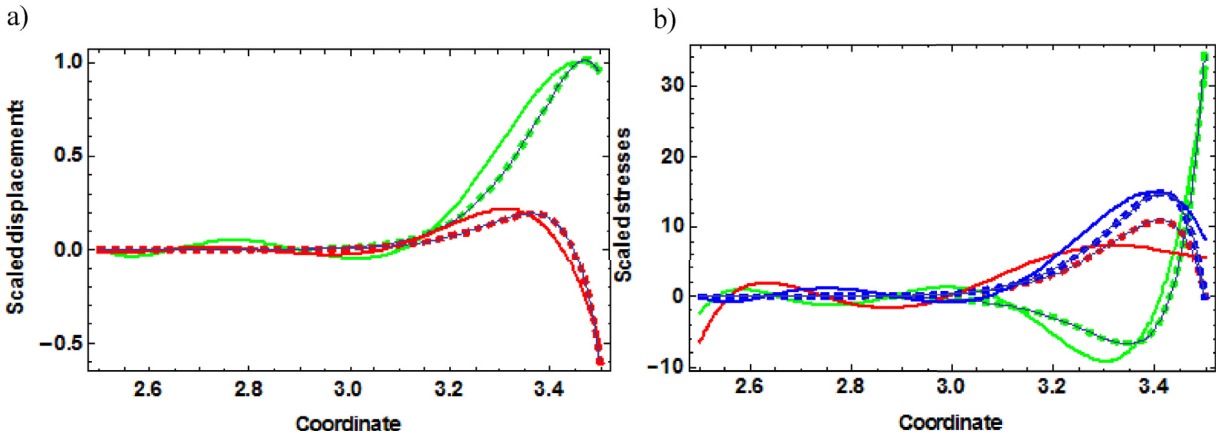

Fig. 20. Scaled displacements (a) and stresses (b), $\Omega = 10.0$, $k_R = 23.693$, Rayleigh branch Solid/dashed lines: approximations $N = 6/N = 7$, thin lines: exact solution.

branch is $k_R = 23.693$, whereas the six-term approximation gives $k_R = 22.412$. Nevertheless, the presentation of the field variables is qualitatively the same and quantitatively not too different. The wave is localised at the outer surface stronger, that at $\Omega = 5.0$, and there is a good correspondence of these profiles to those presented in Figs. 2e and 3e in Ref. [7].

5.3. *The 'symmetric' and 'anti-symmetric' high-order branches*

We conclude the analysis of field variables by their further inspection at $\Omega = 2.0$. As seen in Fig. 11, two branches exist at this frequency besides the Rayleigh one. In a straight layer, the lower branch belongs to the family of anti-symmetric waves. It may also be referred to as the 'Timoshenko branch', because it is predicted by the Timoshenko beam theory. The middle branch belongs to the family of symmetric waves in a straight layer.

In Fig. 21, displacements and stresses for the 'Timoshenko branch' are presented. As shown in the previous sub-section, $\Omega = 2.0$ lies outside the validity range of the three-term model, so we consider only $N = 6$ and $N = 7$ approximations along with the exact solution, which perfectly agree with each other and yield the wavenumber $k_T = 0.999$. In a straight layer, distribution of the axial displacements $\tilde{U}_T(r)$ and shear stresses $\tilde{\sigma}_{r\theta T}(r)$ would be perfectly symmetric with respect to the centreline $r = 3$, while distribution of the radial displacements $\tilde{V}_T(r)$ and both normal stresses $\tilde{\sigma}_{rrT}(r)$ and $\tilde{\sigma}_{\theta\theta T}(r)$ would be anti-symmetric. As seen in Fig. 21, the dominant type of displacement is radial, and the function $\tilde{V}_T(r)$ is non-linear. Therefore, the shape of displacement field has departed from that in a straight layer. However, the shapes of stress distribution feature the expected evenness/oddness – although the dominant normal axial stresses are much larger at the inner surface of a layer, than on its outer surface. The shear stresses are also rather large, as expected in the 'Timoshenko branch' near its cut-on frequency in a straight layer.

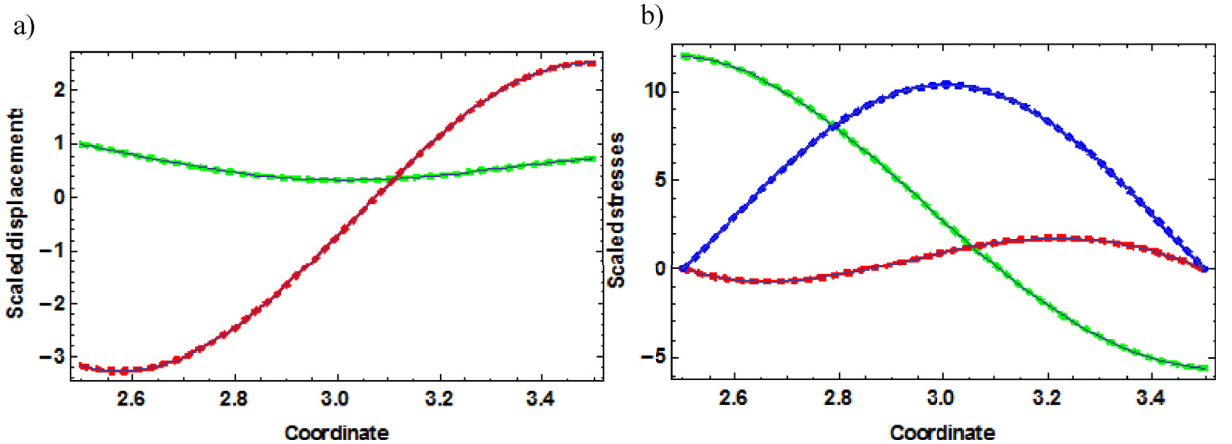

Fig. 21. Scaled displacements (a) and stresses (b), $\Omega = 2.0$, $k_T = 0.999$, Timoshenko branch Solid/dashed lines: approximations $N = 6/N = 7$, thin lines: exact solution.

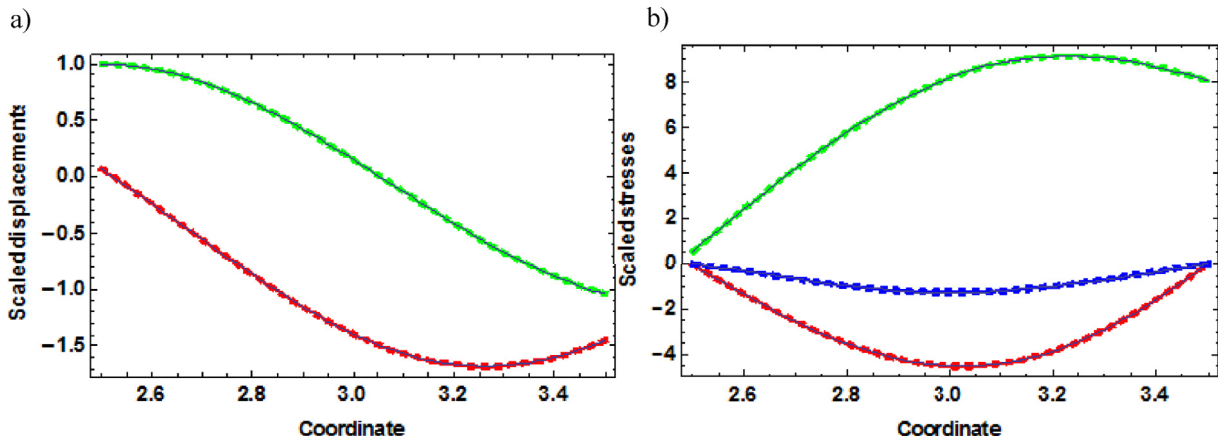

Fig. 22. Scaled displacements and stresses, $\Omega = 2.0$, $k_M = 2.497$, middle branch Solid/dashed lines: approximations $N = 6/N = 7$, thin lines: exact solution.

The middle branch at $\Omega = 2.0$ is characterised by the wavenumber $k_M = 2.497$ in exact formulation (and the same value in $N = 6$ and $N = 7$ approximations). As seen in Fig. 22, 'mixing' of symmetric and anti-symmetric components is also rather pronounced and the shape of the axial displacements $\tilde{U}_M(r)$ looks more anti-symmetric with respect to the centreline than symmetric as it should have been in a straight layer. The second largest stress component is the radial normal stress $\tilde{\sigma}_{rrM}(r)$, and its distribution agrees with the evenness typical for a straight layer. The strong coupling of symmetric and anti-symmetric components in these two waves at $\Omega = 2.0$may be attributed to the veering phenomenon between the Timoshenko and the middle branches seen in Fig. 11.

6. Conclusions

A hierarchy of novel reduced-order models of wave propagation in an elastic layer of constant curvature and thickness is formulated. These models provide a new family of polynomial approximations to the dispersion relation and corresponding approximations to the field, which have high accuracy, particularly in resolving the surface waves, which are dominant features of the solution.

The generalised Galerkin method is proved to be superior over the conventional simplified approach of taking a linear combination of Legendre polynomials (or any other complete set of orthogonal functions), and integrating over the thickness of a layer after an elementary multiplication. The traction-free boundary conditions are taken into account due to the variational essence of the method, and this feature significantly accelerates its convergence and ensures the match between the exact and the approximate cut-on frequencies.

A useful feature of the proposed novel reduced-order models is that a determination of their accuracy, by means of residuals, can be carried out analytically in terms of simple known functions. In particular, the field values are exact on a set of points spread over the thickness of the layer, so that the method in effect gives the field as an interpolating function between these points, at which there is no error. The residual analysis performed in the paper confirms that, as soon as enough coordinate functions are included to resolve the smallest length-scale in the solution, the convergence of the generalised Galerkin method is exponentially fast.

References

[1] J.D. Achenbach, *Wave Propagation in Elastic Solids* Amsterdam, North-Holland, The Netherlands, 1973.
[2] K.F. Graff, Wave Motion in Elastic Solids, Dover, New York, 1975.
[3] D.C. Gazis, Exact analysis of the plane-strain vibrations of thick-walled hollow cylinders, J. Acoust. Soc. Am. 30 (1958) 786–794.
[4] P. Chidamparam, A.W. Leissa, Influence of centreline extensibility on the in-plane free vibrations of loaded circular arches, J. Sound Vib. 183 (1995) 779–795.
[5] S.J. Walsh, R.G. White, Vibrational power transmission in curved beams, J. Sound Vib. 233 (2000) 455–488.
[6] S.V. Sorokin, C.J. Chapman, A hierarchy of high-order theories for symmetric modes in an elastic layer, J. Sound Vib. 333 (2014) 3505–3521.
[7] C.J. Chapman, S.V. Sorokin, A class of reduced-order models in the theory of waves and stability, Proc. R. Soc. A 472 (2016), 20150703.
[8] V.A. Postnov, *Numerical Methods in Naval Architecture* Sudostroenie, 1979. Leningrad (in Russian).
[9] A.P. Filin, Applied Mechanics of Deformable Solids, vol. II, Nauka, Moscow, 1982 (in Russian).
[10] D. Gottlieb, S.A. Orszag, Numerical Analysis of Spectral Methods, SIAM, Philadelphia, 1977.
[11] O.C. Zienkievicz, The Finite Element Method: its Basis and Fundamentals, sixth ed., Elsevier, Amsterdam, 2005.
[12] C.L. Dym, I.H. Shames, Solid Mechanics: a Variational Approach, Augmented Edition, Springer, New York, 2013.
[13] C.J. Chapman, S.V. Sorokin, The deferred limit method for long waves in a curved waveguide, Proc. R. Soc. A 473 (2017), 20160900.
[14] Lord Rayleigh, Theory of Sound, second ed., vol. II, Dover, New York, 1945.